

3-D Slope Shape Sensing by Laser Range Finder with 4-DOF Sensor Movable Unit

Toyomi Fujita and Toshinori Yoshida

Abstract—The authors have developed a measurement system which consists of a laser range finder with four degrees of freedom arm-type sensor movable unit for a tracked vehicle. The mechanism of the arm-type sensor movable unit enables the sensor to change vertical position and rotate around the roll-axis and pitch-axis. It is thereby possible to perform sensing of rough terrain at equal interval and complex shape such as deep downward slope without occlusion. In this study, we take into account the orientation of the vehicle and employ three-dimensional shape sensing of the front upward steps and front and lateral downward steps by the tracked vehicle equipped with presented measurement system. The experimental results demonstrate the effectiveness of the proposed measurement system.

Index Terms—Laser Range Finder(LRF), 3-D Shape Sensing, Arm-type Sensor Movable Unit, Tracked Mobile Robot.

I. INTRODUCTION

A 3-D shape sensing is a very important function for a tracked vehicle robot to give precise information as possible to operators and to move working field efficiently. A laser range finder (LRF) is widely used for a 3-D sensing because it can detect wide area fast and can obtain 3-D information easily. Some 3-D sensing systems with the LRF have been presented in earlier studies[1][2][3]. In those measurement systems, multiple LRF sensors are installed in different directions[4], or a LRF is mounted on a rotatable unit[5][6]. However, it is still difficult for those systems to do sensing more complex terrain such as valley, deep hole, inside the gap, or steep downward slope due to occlusions. As the other related work, for example, [7] proposed the combination of 2-D LRF and stereo vision for 3-D sensing. This method, however, increases the cost of sensing system.

In the previous study, the authors have proposed a new type of LRF sensing system that is able to sense 3-D shape of such a more complex terrain: valley, deep hole, inside the gap [8]. The system has a 3-DOF arm-type sensor movable unit which can be mounted on a tracked vehicle robot. A LRF is installed at the end of the unit in this sensing system. The sensor can change position and orientation in a movable area of the arm unit and face at a right angle according to a variety of configuration. This system is, therefore, capable of avoiding occlusions for such a complex terrain and sense more accurately.

In addition, this sensing system is able to change the height of the LRF by keeping its orientation flat for efficient sensing. In this way, the height of LRF can be changed at equal interval by lifting it up and down vertically by the arm-type sensor movable unit. 3-D map can be obtained by combining

Toyomi Fujita is with Faculty of Engineering, Department of Electronics and Intelligent Systems, Tohoku Institute of Technology, Sendai 982-8577, Japan e-mail: t-fujita@tohotech.ac.jp
Toshinori Yoshida is with Celestica Japan.

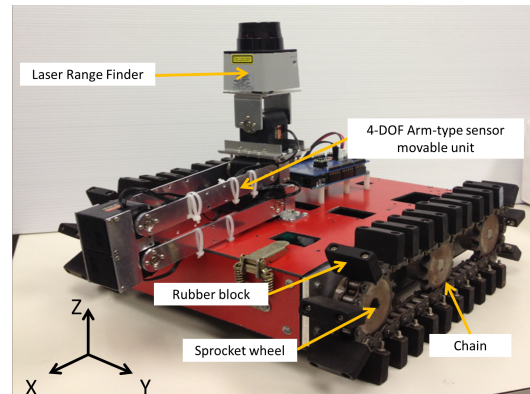


Fig. 1. Tracked Mobile Robot with 4DOF sensor movable unit

2-D maps in individual heights of the LRF. This sensing can avoid a problem on accumulation point in conventional 3-D sensing method by a LRF with a rotating mechanism. However, if a robot is tilted right or left in roll rotation (rotation around the axis to the forward direction), it may be difficult to apply this kind of sensing method because the scanning plane is also tilted with the tilt angle.

Therefore in this study we expand the system to add another revolute joint as a 4-DOF unit so that the robot can keep the LRF flat even on uneven ground. This mechanism enables the robot to sense surround shape of 3-D environment with equal interval even in the condition that the robot is tilted horizontally with the roll rotation in uneven ground.

The aim of this study is to develop expanded system and increase sensing ability of this system even in the situation the robot is tilted. We focus on 3-D shape sensings of upward and downward slopes which are located in front or lateral of the robot as typical examples of complex shape sensing.

This paper describes the expanded mechanism of sensing system with some experimental results. Section II shows the mechanism of the expanded sensing system. The characteristics of 3-D shape sensing by this sensing system is explained in Section III. Section IV describes some fundamental experiment of 3-D shape sensing.

II. ROBOT AND SENSING SYSTEM

A. Tracked Mobile Robot

Figure 1 shows the tracked mobile robot with proposed sensing system. The size of the robot is 350 mm in length, 330 mm in width, and 320 mm in height. The total weight is approximately 11 kg.

B. 4-DOF Sensor Movable Unit

The expanded sensing system by 4-DOF sensor movable unit is mounted on the robot as shown in Fig. 1. This unit

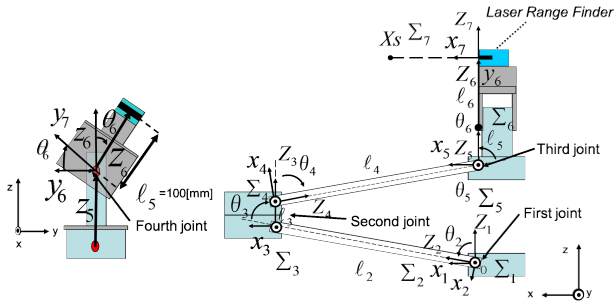


Fig. 2. Sensor Coordinate System

consists of two links, three revolute joints which can rotate around Y-axis, and additional fourth joint rotating around X-axis. The first and second joints and the second and third joints are connected by a link respectively. Two servomotors are used for the second joint to make LRF flat when it is fully down.

The coordinate systems for the joints and sensor is shown in Fig. 2. The coordinate system Σ_1 is set at the base of the arm and Σ_2 , Σ_3 and Σ_4 , Σ_5 , and Σ_6 are corresponds to the first, second, third, and fourth joints respectively. The sensor coordinate system is represented by Σ_7 .

In this system, the robot can obtain 3-D sensing positions from the sensor data of the LRF. When the distance is d_s at a scan angle θ_s by LRF, the 3-D measurement position vector \mathbf{X} in the base coordinate system Σ_1 can be calculated by

$$\begin{pmatrix} \mathbf{X} \\ 1 \end{pmatrix} = {}^1\mathbf{P}_6 {}^6\mathbf{P}_7 \begin{pmatrix} \mathbf{X}_s \\ 1 \end{pmatrix} \quad (1)$$

where \mathbf{X}_s shows a position vector of sensor in the sensor coordinate system Σ_7 :

$$\mathbf{X}_s = d_s (\cos \theta_s, \sin \theta_s, 0)^T. \quad (2)$$

${}^i\mathbf{P}_{i+1}$ ($i = 1, \dots, 6$) shows a homogeneous matrix that represents a transformation between two coordinate systems Σ_i and Σ_{i+1} :

$${}^i\mathbf{P}_{i+1} = \begin{pmatrix} {}^i\mathbf{R}_{i+1} & {}^i\mathbf{T}_{i+1} \\ \mathbf{0}_3^T & 1 \end{pmatrix} \quad (i = 1, \dots, 6) \quad (3)$$

where ${}^i\mathbf{R}_{i+1}$ shows a rotation matrix for the rotation angle θ_{i+1} ; in case of $i = 1, \dots, 4$, it is gives by

$${}^i\mathbf{R}_{i+1} = \begin{pmatrix} \cos \theta_{i+1} & 0 & \sin \theta_{i+1} \\ 0 & 1 & 0 \\ -\sin \theta_{i+1} & 0 & \cos \theta_{i+1} \end{pmatrix}, \quad (4)$$

and ${}^i\mathbf{T}_{i+1}$ shows a translation vector from Σ_i to Σ_{i+1} for the translation l_i on z_i axis:

$${}^i\mathbf{T}_{i+1} = (0, 0, l_i)^T \quad (5)$$

for $i = 1, \dots, 5$ ($l_1 = 0$). $\mathbf{0}_3$ shows a 3×1 zero vector. In case of $i = 6$, ${}^6\mathbf{R}_7$ shows a rotation matrix for the rotation angle θ_6 around X-axis, and ${}^6\mathbf{T}_7$ is a translation vector from Σ_6 to Σ_7 .

C. Control System

Figure 3 shows the control system for this robot. We have used Arduino Mega for the control of the sensor movable unit and tracks driving. This microcomputer board

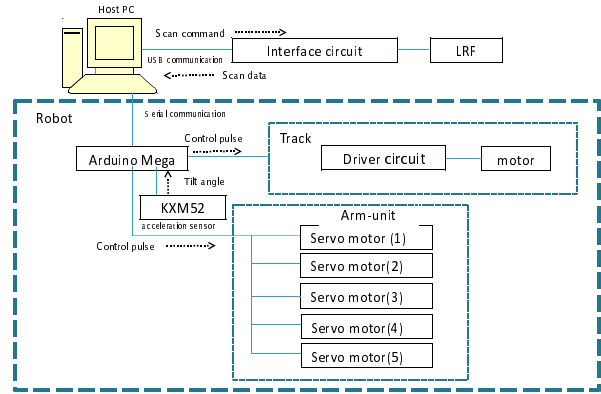


Fig. 3. Control System

receives desired position and orientation of LRF from the host PC, computes desired joint angles of the unit based on received information and the orientation of robot, then sends the control signals corresponding to the joint angles to each motor. The orientation of the robot is detected by 3-axis acceleration sensor: Kionix Inc. KXM52. The board also manages PWM control of each motor for driving track corresponding to the movement command received from the host PC. The LRF sends the scanned data to the host PC when the host PC requests for the sensing data to LRF. The host PC computes 3-D sensing positions from the sensing data of LRF and information of the robot state received from the microcomputer: orientation of the robot and joint angles of the sensor movable unit. We have used MATLAB for the computation and map building from the data.

III. 3-D SHAPE SENSING

This presented sensing system has two major advantages.

One advantage is that the sensing system enable the robot to perform 3-D shape sensing without sparse or dense scanning because this system is able to scan at different heights with equal interval. For example, in case of upward slope located in front of the robot as shown in Fig. 4, presented system can perform 3-D shape sensing by moving LRF up and down with equal interval with keeping its orientation flat to the ground. Specifically, it rotates the first, second, and third joints around Y-axis and move LRF up and down. Also, it rotates the third and fourth joints according to tilt angle of the robot which is detected by acceleration sensor so that the orientation LRF is flat to the ground. Therefore, it can perform 3-D shape sensing of upward slope by scanning in horizontal planes at equal interval.

Another advantage is that this system reduce occlusions in sensings of steep downward slope and valley shape terrain which are located in front and lateral of the robot. For front downward slope, as shown in the left panel of Fig. 5, the sensing without occlusion is possible by holding the angles of the first and second joints and rotating the third joint around Y-axis. In case of lateral downward slope shown in the right panel of Fig. 5, the occlusion may occur due to mechanical limitation of the sensor movable unit. Nevertheless, it can make the measurement area large by locating the LRF high position as possible and rotating the fourth joint around X-axis.

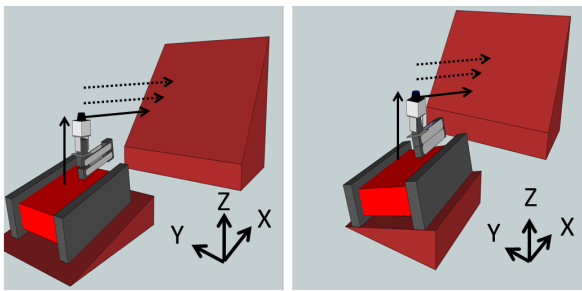


Fig. 4. 3-D shape sensings of upward slope at equal intervals

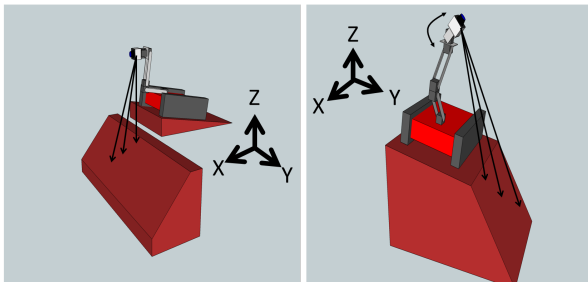


Fig. 5. 3-D shape sensings of downward slope in front (left panel) and lateral (right panel) of the robot

IV. EXPERIMENTS

We have employed experiments for 3-D shape sensing for upward and downward slopes as described in Section III.

A. 3-D Shape Sensing of Front Upward Steps

Upward steps were setup for the experiment of upward slope. Figure 6 shows an overview of experimental setup. The steps were located in front of the robot, at (1150, 0, 310) mm in the global coordinate system which is located as shown in Fig. 6. Each step had 1080 mm in width, 80 mm in length and height. The position of the robot was set so that the origin of the arm-base coordinate system Σ_1 was located at (360, -160, 100) mm. Based on this, three kinds of experiment were proceeded in which the orientation of the robot was changed with upward movement of the LRF by the following manners:

- (1) The rotation angle around X-axis was changed to -15 or -25 degrees as the LRF moved 2.5 mm up. The rotation angle around Y-axis was fixed to be 0 degree.
- (2) The rotation angle around Y-axis was changed to -15 or -25 degrees as the LRF moved 2.5 mm up. The rotation angle around X-axis was fixed to be 0 degree.
- (3) The combination of rotation angles around X-axis and Y-axis was changed to $\{0, -15\}$, $\{-20, -15\}$, $\{-20, -25\}$, or $\{0, -25\}$ degrees as the LRF moved 2.5 mm up in turn.

In each orientation, LRF was kept to be flat to the ground and moved upward. The shape sensing in a horizontal plane was performed at every heights by 0.5 mm interval.

In this experiment, some feature points in the environment were set as reference points to evaluate sensing accuracy. Figure 7 shows the reference points at which positions were represented in the global coordinate system.

Figure 8 shows the result of sensing based on the above experiment (3); the blue lines show the obtained shape and

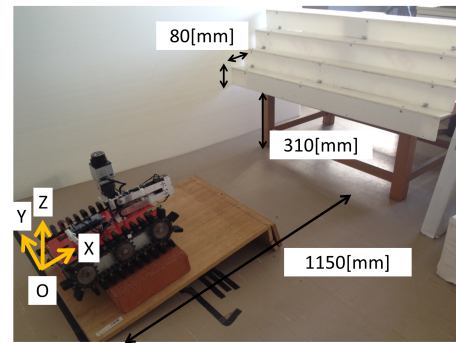


Fig. 6. Experimental setup for 3-D shape sensing of front upward steps

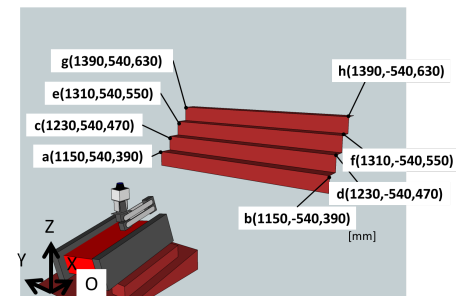


Fig. 7. Reference points for 3-D shape sensing of front upward steps

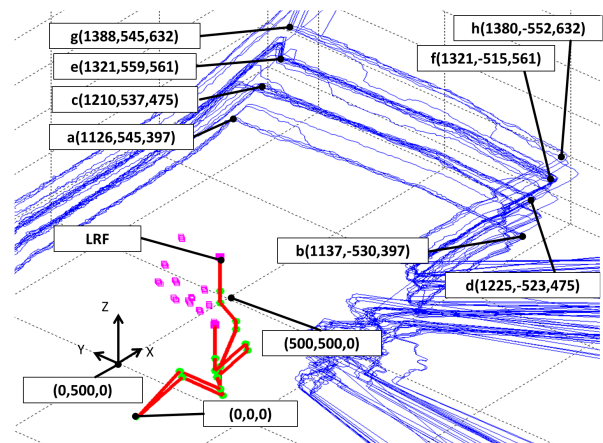


Fig. 8. 3-D shape sensing result of front upward steps with measured reference points (unit:[mm])

measured position values of reference points are also described. We can see that almost accurate shape was obtained. The position errors on reference points were acceptable so that the robot figures out the environment: for example, the position error was (24, 5, 7) mm, its ratio was (2.1, 0.9, 2.0) %, on the point *a*; (13, 10, 7) mm, (1.1, 2.0, 2.0) %, on the point *b*; and the maximum error was 5.0 % on Y-axis of the point *f*.

Table I shows measured distances and errors on reference points for the above experiments. In case of the experiment (1), the average of the error was 0.6 %, the maximum error was 1.6 % on the point *f*, and the minimum error was 0.02 % on the point *c*. In case of the experiment (2), the average of the error was 0.7 %, the maximum error was 2.0 % on the points *e* and *f*, and the minimum error was 0.03 % on the point *a*. In case of the experiment (3), the average of the error was 0.7 %, the maximum error was 1.4 % on the

TABLE I
 MEASURED DISTANCES AND ERROR RATIOS ON REFERENCE POINTS FOR FRONT UPWARD STEPS

experiment	(1)			(2)		(3)	
rotation angle around X	0 degree			-15 or -25 degrees		0 or -20 degrees	
rotation angle around Y	-15 or -25 degrees			0 degree		-15 or -25 degrees	
point	actual (mm)	measured (mm)	error (%)	measured (mm)	error (%)	measured (mm)	error (%)
a	1329.0	1335.7	0.5	1328.5	0.03	1312.4	1.2
b	1329.0	1338.1	0.6	1327.7	0.1	1315.8	1.0
c	1423.2	1422.9	0.02	1421.4	0.1	1406.4	1.2
d	1423.2	1426.8	0.3	1431.8	0.6	1414.1	0.6
e	1492.8	1510.3	1.2	1517.0	2.0	1540.2	1.4
f	1492.8	1517.3	1.6	1515.7	2.0	1524.8	0.3
g	1618.8	1617.4	0.09	1622.5	0.2	1619.6	0.05
h	1618.8	1630.4	0.7	1629.1	0.6	1615.1	0.2
average			0.6		0.7		0.7

point *e*, and the minimum error was 0.05 % on the point *g*. In all experiments, the average of the error was within 1 %, so these results show that accurate 3-D shape sensing is possible for the robot to understand surrounding environment by the presented sensing system.

B. 3-D Shape Sensing of Front Downward Steps

Downward steps were setup for the experiment of downward slope. Figure 9 shows an overview of experimental setup. The steps were located in front of the robot, at (770, 0, -55) mm in the global coordinate system. Each step had 1080 mm in width, 80 mm in length and height. The position of the robot was set so that the origin of the arm-base coordinate system Σ_1 was located at (400, 0, 100) mm. The orientation of the robot was set to the -15 degrees as the rotation angle around Y-axis and 0 degree as the angle around X-axis. The position of LRF was fixed at (531, 0, 432) mm and the angle of the third joint θ_5 was changed from 1 degree to 90 degrees by 1 degree. The measurement was performed in each orientation of LRF. As the previous experiment, some reference points were given and the error of measured distance was computed for each point. The positions of the reference points in the global coordinate system are described in Fig. 10.

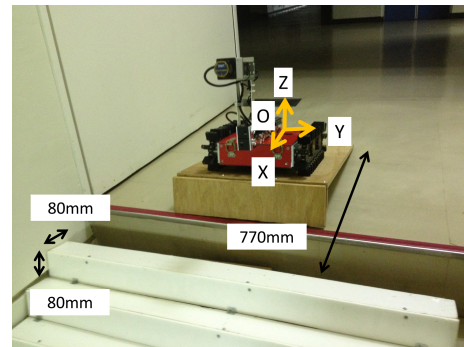


Fig. 9. Experimental setup for 3-D shape sensing of front downward steps

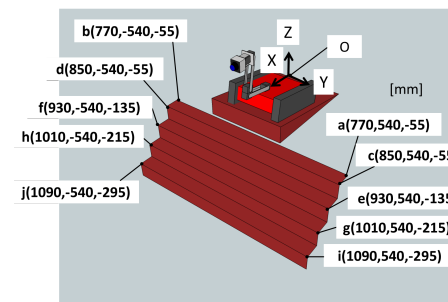


Fig. 10. Reference points for 3-D shape sensing of front downward steps

Figure 11 shows the result of sensing: the blue lines show the obtained shape and measured position values of reference points are also described. The position errors on reference points were acceptable so that the robot figures out the environment; for example, (5, 4, 1) mm, the ratio was (0.6, 0.7, 2.0) %, on the point *a*; and (11, 4, 1) mm, (1.4, 0.7, 2.0) %, on the point *b*. The maximum error was 19.3 % on Z-axis of the points *e* and *f*.

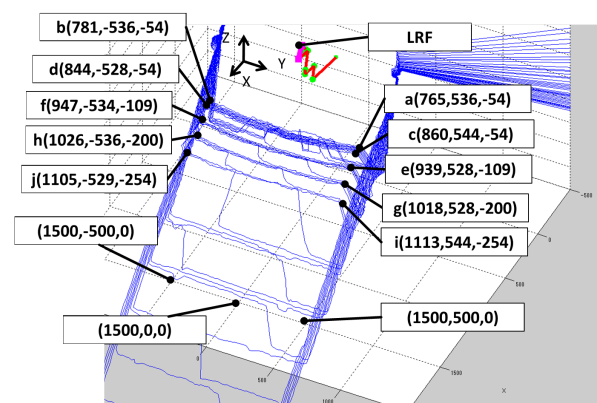


Fig. 11. 3-D shape sensing result of front downward steps with measured reference points (unit:[mm])

Table II shows measured distances and errors on reference points. The maximum error was 1.1 % on the point *d* and the minimum error was 0.04 % on the point *j*. The average of measured distance was 0.6 %, so this result shows that accurate 3-D shape sensing without occlusion is possible for the robot to understand surrounding front downward environment by the presented sensing system.

C. 3-D Shape Sensing of Lateral Downward Steps

Downward steps were setup for the experiment of downward slope as well as previous experiment. Figure 12 shows an overview of experimental setup. The steps were located in the left side of the robot, at (0, 120, -55) mm in the global coordinate system. The position of the robot was set so that

the origin of the arm-base coordinate system Σ_1 was located at (0, -160, 100) mm. The following two kinds of experiment were proceeded in which the combinations of the orientation of robot and the position of LRF were set as follows:

- (1) The rotation angle of the robot around X-axis was set

TABLE II
MEASURED DISTANCES AND ERROR RATIOS ON REFERENCE POINTS FOR
FRONT DOWNWARD STEPS

point	actual (mm)	measured (mm)	error (%)
a	942.1	935.6	0.6
b	942.1	948.8	0.7
c	1008.5	1019.0	1.0
d	1008.5	997.0	1.1
e	1083.8	1082.8	0.1
f	1083.8	1092.6	0.8
g	1165.3	1164.1	0.1
h	1165.3	1174.7	0.8
i	1251.7	1264.6	1.0
j	1251.7	1251.2	0.04
average			0.6

to 25 degrees and the LRF was located at (0, -418, 637) mm.

- (2) The rotation angle of the robot around X-axis was set to -25 degrees and the LRF was located at (0, 85, 489) mm.

In each combination, the angle of the fourth joint θ_6 was changed from 90 degrees to 0 degree by -1 degree and the LRF was performed sensing in each orientation. As the previous experiments, some reference points were given and the error of measured distance was computed for each point. The positions of the reference points in the global coordinate system are described in Fig. 13.

Figure 14 shows the result of sensing based on the above experiment (2); the blue lines shows the obtained shape and measured position values of reference points are also described. Although almost accurate shape was obtained, the measurement was not performed in a part of area due to occlusion. The position errors on reference points were, for example, (8, 3, 1) mm, the ratio was (1.4, 2.5, 2.0) %, on the point *b*; and (8, 2, 1) mm, (1.4, 1.0, 2.0) %, on the point *d*. With respect to the maximum error of the position, it was 5.7 % on Y-axis of the point *j* in the experiment (2) and 7.2 % of the points *b* and *d* in the experiment (1).

Table III shows measured distances and errors on reference points for each experiment. In case of the experiment (1), the average of the error was 1.3 %, the maximum error was 2.5 % on the point *b*, and the minimum error was 0.1 % on the point *d*. In the experiment (1), however, the robot was not able to obtain enough 3-D shape and the data on reference points were insufficient because occlusions occurred in lateral downward area. The points at which the measurement was not made were denoted by a line in Table III. In case of the experiment (2), the average of the error was 2.2 %, the maximum error was 3.0 % on the point *i*, and the minimum error was 0.6 % on the point *f*. The measurement was not made on the points *a*, *c*, and *e* because these were in the outside of measurement region of LRF. Nevertheless, these results show that accurate 3-D shape sensing is possible for the presented sensing system to understand surrounding lateral downward environment, where conventional sensing systems were never able to measure.

V. CONCLUSIONS

This paper presented a 3-D shape sensing system by LRF with 4-DOF sensor movable unit. Using the sensor movable unit, 3-D shape sensing by flat scanning is possible even in the condition that the robot is tilted. Experiments for

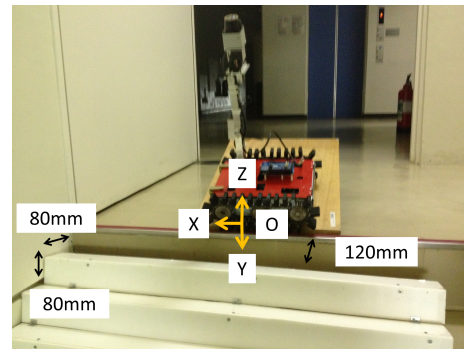


Fig. 12. Experimental setup for 3-D shape sensing of lateral downward steps

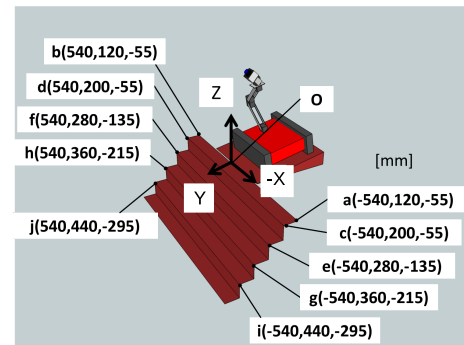


Fig. 13. Reference points for 3-D shape sensing of lateral downward steps

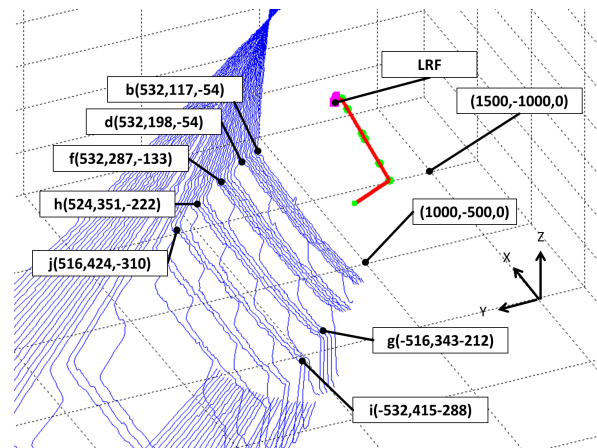


Fig. 14. 3-D shape sensing result of lateral downward steps with measured reference points (unit:[mm])

front upward steps showed the effectiveness of this sensing. In addition, this sensing system is able to perform 3-D shape sensing of surrounding front and lateral downward environment with less occlusion where conventional sensing systems were not able to measure. As future work, we plan to consider a method for more flexible sensing by changing the position and orientation of the sensor according to conditions in surrounding environment such as terrain.

REFERENCES

- [1] M. Hashimoto, Y. Matsui, and K. Takahashi, "Moving-object tracking with in-vehicle multi-laser range sensors," *Journal of Robotics and Mechatronics*, vol. 20, no. 3, pp. 367-377, 2008.
- [2] T. Ueda, H. Kawata, T. Tomizawa, A. Ohya, and S. Yuta, "Mobile SOKUIKI Sensor System-Accurate Range Data Mapping System with Sensor Motion," in *Proceedings of the 2006 International Conference on Autonomous Robots and Agents*.

TABLE III
MEASURED DISTANCES AND ERROR RATIOS ON REFERENCE POINTS FOR
LATERAL DOWNWARD STEPS

experiment		(1)		(2)	
rotation angle around X		25 degrees		-25 degrees	
point	actual (mm)	measured (mm)	error (%)	measured (mm)	error (%)
a	555.9	—	—	—	—
b	555.9	541.9	2.5	547.4	1.5
c	578.5	—	—	—	—
d	578.5	579.2	0.1	570.2	1.4
e	623.1	—	—	—	—
f	623.1	—	—	618.9	0.6
g	623.7	—	—	654.9	4.2
h	623.7	—	—	668.6	2.2
i	756.5	—	—	733.6	3.0
j	756.5	—	—	736.3	2.7
average			1.3		2.2

- [3] K. Ohno and S. Tadokoro, "Dense 3D map building based on LRF data and color image fusion," in *2005 IEEE/RSJ International Conference on Intelligent Robots and Systems, 2005.(IROS 2005)*, 2005, pp. 2792–2797.
- [4] J. Poppinga, A. Birk, and K. Pathak, "Hough based terrain classification for realtime detection of drivable ground," *Journal of Field Robotics*, vol. 25, no. (1-2), pp. 67–88, 2008.
- [5] A. Nuchter, K. Lingemann, and J. Hertzberg, "Mapping of rescue environments with kurt3d," in *In Proc. IEEE SSRR 2005*, 2005, pp. 158–163.
- [6] Z. Nemoto, H. Takemura, and H. Mizoguchi, "Development of Small-sized Omni-directional Laser Range Scanner and Its Application to 3D Background Difference," in *Industrial Electronics Society, 2007. IECON 2007. 33rd Annual Conference of the IEEE*, 2007, pp. 2284–2289.
- [7] L. Iocchi, S. Pellegrini, and G. Tipaldi, "Building multi-level planar maps integrating LRF, stereo vision and IMU sensors," in *Safety, Security and Rescue Robotics, 2007. SSRR 2007. IEEE International Workshop on*, 2007, pp. 1–6.
- [8] T. Fujita and Y. Kondo, "3D Terrain Measurement System with Movable Laser Range Finder," in *2009 IEEE International Workshop on Safety, Security, and Rescue Robotics (SSRR 2009)*, 2009.